iScience

CellPress
OPEN ACCESS

Article

All-polymer wearable thermoelectrochemical cells harvesting body heat

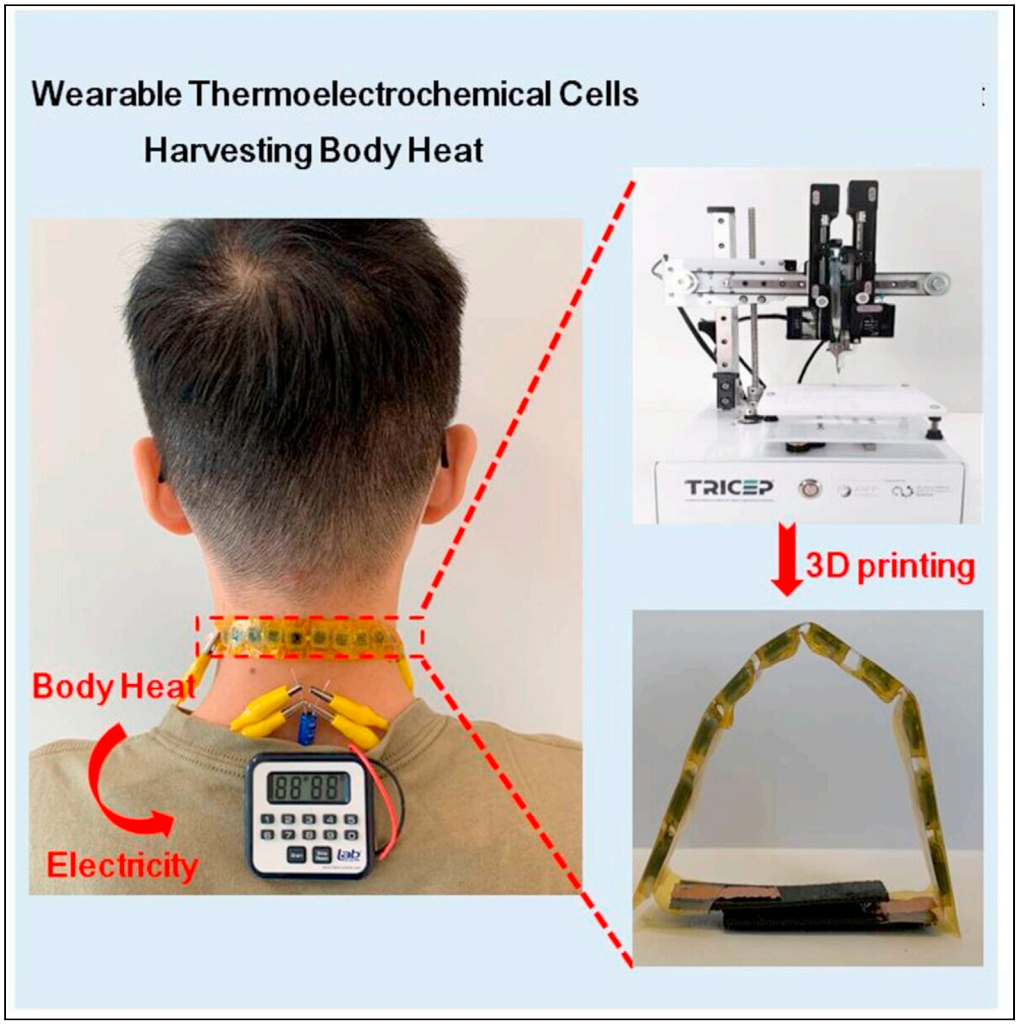

Shuai Zhang, Yuetong Zhou, Yuqing Liu, Gordon G. Wallace, Stephen Beirne, Jun Chen

gwallace@uow.edu.au (G.G.W.)
junc@uow.edu.au (J.C.)

Highlights

A compatible high electrical conductivity polymer film works as underlying substrate

3D printable polymer ink with suitable rheological properties

A serial 18 pairs of n-p devices charged supercapacitor to power a lab timer

3D-printed all-polymer electrode thermocell device for harvesting body heat

Zhang et al., iScience 24, 103466
December 17, 2021
https://doi.org/10.1016/j.isci.2021.103466

iScience

CellPress
OPEN ACCESS

Article

All-polymer wearable thermoelectrochemical cells harvesting body heat

Shuai Zhang,[1] Yuetong Zhou,[1] Yuqing Liu,[2] Gordon G. Wallace,[1,*] Stephen Beirne,[1] and Jun Chen[1,3,*]

SUMMARY

Wearable thermoelectrochemical cells have attracted increasing interest due to their ability to turn human body heat into electricity. Here, we have fabricated a flexible, cost-effective, and 3D porous all-polymer electrode on an electrical conductive polymer substrate via a simple 3D printing method. Owing to the high degree of electrolyte penetration into the 3D porous electrode materials for redox reactions, the all-polymer based porous 3D electrodes deliver an increased power output of more than twice that of the film electrodes under the same mass loading using either n-type or p-type gel electrolytes. To realize the practical application of our thermocell, we fabricated 18 pairs of n-p devices through a series connection of single devices. The strap shaped thermocell arrangement was able to charge up a commercial supercapacitor to 0.27 V using the body heat of the person upon which it was being worn and in turn power a typical commercial lab timer.

INTRODUCTION

With the rapid development of next-generation wearable electronics, such as portable devices and soft electric devices, there is strong demand for lightweight, wearable, and environmentally friendly energy devices, such as piezoelectric nanogenerators, thermoelectric generators and thermoelectrochemical cells (Dargusch et al., 2020; Shi et al., 2020; Khan et al., 2021; Jia et al., 2021; Tian et al., 2019; Zhang et al., 2021). Human body heat is an accessible, relatively consistent, and environmentally friendly power source with a temperature difference (ΔT) between human skin and ambient environment (Oh et al., 2016; Zhong et al., 2014). The most convenient strategy to use this low-grade thermal energy is to convert thermal to electricity. Conventional thermoelectric generators (TEGs) utilizing the Seebeck effect are mostly dependent on thermoelectric (TE) materials such as semiconductors or electrical conducting polymers. These TE materials are either expensive or exhibit low Seebeck Coefficient (S_e, $S_e = \Delta V/\Delta T$, the open voltage is ΔV, and the temperature difference is ΔT) in the range of several hundreds of μVK^{-1} (Khan et al., 2016; Bux et al., 2010), limiting their application in wearable electronics for harvesting of low-grade body heat (Khan et al., 2016). Alternatively, thermoelectrochemical cells (also called thermogalvanic cells or thermocells) can generate a larger thermal voltage, which is caused by a temperature-dependent entropy change during the electron transfer process between the redox couples and the electrode (Liu et al., 2021; Romano et al., 2012). The simple device structure, the low-cost of electrode and electrolyte materials, and the relatively large S_e has made thermoelectrochemical cells a promising candidate to efficiently harvest low-grade body heat.

The performance of thermoelectrochemical cells (TEC) is greatly dependent on the electrode materials employed (Dupont et al., 2017; Hu et al., 2010; Im et al., 2014). Electrodes in wearable thermoelectrochemical cells should meet a number of requirements including low cost, large surface area, high electrical conductivity, extraordinary flexibility, porous architecture, and high thermal conductivity (Dupont et al., 2017; Hu et al., 2010; Im et al., 2016). In previous studies, platinum (Pt) electrodes have been conceived as an ideal electrode material for wearable thermocells because of the high electrical conductivity and high catalytic activity of the material (Im et al., 2016; Zhou et al., 2021). However, the high-cost of platinum greatly limits its use as a commercially available electrode material. Carbon based materials, including carbon cloth, carbon nanotubes (CNTs) and graphene (Romano et al., 2013), could provide large active surface areas and high electrical conductivities, which lead to large numbers of reaction sites and fast electron transfer kinetics for the redox couples. These advantages could increase the obtainable current density of thermocell devices (Kang et al., 2012). However, there are limitations in the processing of these carbon materials into a

[1]Intelligent Polymer Research Institute and ARC Centre of Excellence for Electromaterials Science, University of Wollongong, Wollongong, NSW 2522, Australia

[2]State Key Laboratory of Electronic Thin Film and Integrated Devices, University of Electronic Science and Technology of China, Chengdu 610054, PR China

[3]Lead contact

*Correspondence: gwallace@uow.edu.au (G.G.W.), junc@uow.edu.au (J.C.)

https://doi.org/10.1016/j.isci.2021.103466

homogeneous dispersion and subsequebtly in making electrodes from such dispersions (Romano et al., 2013; Liu et al., 2020).

Conducting polymers (CPs) are promising materials for wearable electronics because of their high electrical conductivity, intrinsic flexibility, relative low-cost, light weight, and ease of preparation (Liu et al., 2020). The suitability of CPs as electrode materials for thermocell devices has been investigated in recent years. For example, poly (3,4-ethylenedioxythio-phene): polystyrenesulfonate (PEDOT:PSS), one of the most popular CPs, has been reported to provide attractive alternative to platinum electrodes (Yuk et al., 2020). Owing to a low charge transfer resistance, films of PEDOT:PSS showed performance that was comparable to carbon-based materials for a thermocell application (Wang et al., 2020). However, current PEDOT:PSS electrodes are generally in a thin film form prepared via techniques including drop-casting (Wang et al., 2020), ink-jet printing (Perinka et al., 2013), and screen printing (Sinha et al., 2017), in which the penetration of electrolyte, ion transfer rate and ion accessible surface area are greatly limited. As a result, it is hard to further increase the performance (especially the current & power output) of the thermocell using these electrode configurations. To address this issue, a PEDOT:PSS electrode with a 3D porous structure is required.

Herein, we developed a PEDOT:PSS-based ink with rheological properties (in terms of viscosity, shear thinning, and shear yielding) desirable for 3D printing, which allows the direct printing of PEDOT:PSS with controlled line spacing and interlayer spacing porosity to produce well defined structures. The printed porous PEDOT:PSS electrode with an interaxial design (the printed direction rotated through 45° for each successive layer) could provide surface and cross-sectional area, which enables a high degree of electrolyte penetration into the electrode for redox reactions to occur and give rise to increased current, open voltage, and power density. Meanwhile, we also find that a thin PEDOT:PSS film prepared via drop-casting technique, can be integrated with the printed structure to act as the current collector. This configuration exhibits superior performance in comparison to conventionally sputter coated platinum films in terms of endurance over repeated bending cycles and thermoelectrochemical performance (i.e., current & power output). Hence, an all polymer-based electrode with a 3D printed porous PEDOT:PSS structure integrated with a thin PEDOT:PSS film, for thermocell applications has been successfully fabricated. In addition, the prepared all polymer electrodes display excellent and comparable performance in both n-type (PVA-$FeCl_{2/3}$) and p-type (CMC-$K_{3/4}Fe(CN)_6$) gel electrolytes, so a matched pair of n-p cell was efficiently achieved. To demonstrate the practical application of our thermocell, we also fabricated 18 pairs of n-p devices connected in series arranged in a strap shaped thermocell assembly. The assembled device was able to charge up a commercial supercapacitor to 0.27 V using the body heat of the person upon which it was being worn and in turn power a typical commercial lab timer.

RESULTS AND DISCUSSION

Selection criteria of electrical conductive substrates for 3D printing of electrode materials

It is widely known that electrode materials in energy devices are usually coated on a conductive thin film (*e.g.* platinum, gold, stainless steel, etc), which act as the current collector to collect electrical current generated at the electrodes (Antiohos et al., 2011). In most thermocell studies, sputter coated platinum electrodes have been used due to the high electrical conductivity and high catalytic activity behaviour that platinum provides (Dupont et al., 2017). However, in wearable applications, devices are usually bent over large angles (close to 180°) or even twisted as they conform to the wearer during movement (Im et al., 2014; Liu et al., 2020; Yang et al., 2016). Here we found sputter coated platinum (Pt) is not stable under these conditions and would peel off from the substrate after 10 bending cycles (see Figure 1A). As a result, the thermoelectrochemical performance (*i.e.,* Seebeck coefficient, current density, and power density for short term & long term) in both n-type and p-type electrolyte is greatly affected as shown in Figures 1B, 1C, and S1. Hence, sputter coated Pt is not a stable conductive substrate upon which to integrate 3D printed active electrode materials for wearable thermocell devices. To address this problem, we utilized a thin PEDOT:PSS film (2 mg cm^{-2}) as an alternative cast conductive substrate for 3D printing. This thin PEDOT:PSS film is reported as a flexible and electrically conductive electrode material for thermocell, which can be easily fabricated via a simple drop-coating technique (by unifying the concentration and then controlling the volume of the drop per unit area)(Liu et al., 2020; Wijeratne et al., 2017). After an optimization study of PEDOT:PSS films with mass loadings ranging of from 0.5 mg cm^{-2} to 4 mg cm^{-2} (see Figures S2A and S2B and thickness in Table S1), the thermocell device made from 2 mg cm^{-2} PEDOT:PSS film electrode delivered the highest thermoelectrochemical performance in both n and p type electrolytes. The recorded

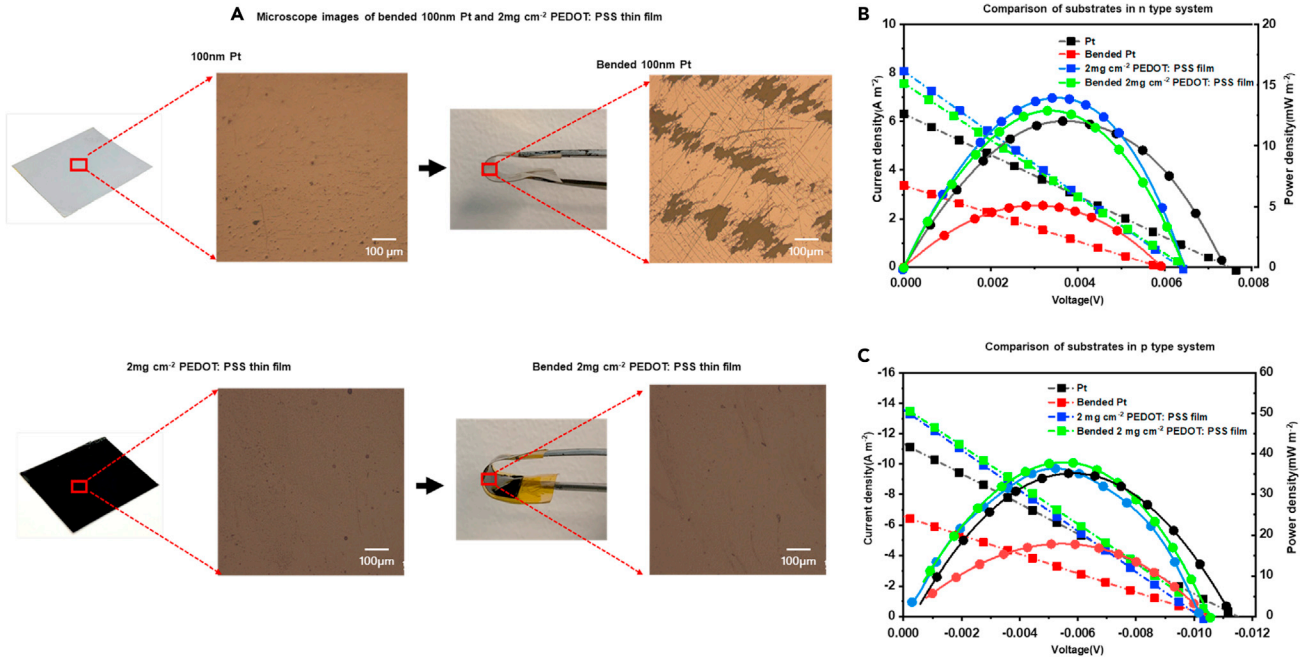

Figure 1. Selection criteria of electrical conductive substrates for 3D printing of electrode materials

(A) Microscope images of 100 nm Pt and 2 mg cm^{-2} PEDOT: PSS film before and after bended (scale bar size is 100μm).

(B) TEC performance: current & power versus voltage of the devices made from 100 nm Pt, bended 100 nm Pt, 2 mg cm^{-2} PEDOT: PSS film and 2 mg cm^{-2} bended PEDOT: PSS film in n-type electrolyte (ΔT = 10°C).

(C) TEC performance: current and power versus voltage of the devices made from 100 nm Pt, bended 100 nm Pt, 2 mg cm^{-2} PEDOT: PSS film and 2 mg cm^{-2} bended PEDOT: PSS film in p-type electrolyte (ΔT = 10°C).

performance was compatible with that observed from a device made from 100 nm Pt electrodes (Figures 1B and 1C). Meanwhile, the performance of thermocells made with PEDOT:PSS films were almost the same after multiple bending cycles. Therefore, the PEDOT:PSS film with a mass loading of 2 mg cm^{-2} was selected for the cast conductive substrate.

Preparation of printable PEDOT: PSS ink

To prepare homogenous printable ink dispersions, a commercial PEDOT:PSS pellets was used in this study. PEDOT:PSS pellets and diethylene glycol (DEG) were dispersed in deionized (DI) water with a weight ratio of (PEDOT:PSS):DEG = 1:1.86 and homogenized by a Thinky Mixer (see experimental details and Figure S3). Here, DEG is used as a secondary dopant to enhance the electrical conductivity (increasing from 3.2 S cm^{-1} to 230 S cm^{-1}), as well as to induce accessible microscale pores within resultant PEDOT:PSS films (Liu et al., 2018).

As the concentration of PEDOT:PSS increased, the prepared suspension transformed from liquid state to a gelled and printable state (Figure S4A), a result of the entanglement of PEDOT:PSS fibrils at high concentrations (Yuk et al., 2020). Rheological measurements of the PEDOT:PSS inks demonstrate the transition from low concentration PEDOT:PSS (10 mg mL^{-1} to 50 mg mL^{-1}) with low viscosity (1.75 Pa·s to 2297 Pa·s at 0.01 s^{-1} shear rate) to high concentration PEDOT:PSS (50 mg mL^{-1} to 120 mg mL^{-1}) with high viscosity (2297 Pa·s to 25,148 Pa·s at 0.01 s^{-1} shear rate (Figure S4B). In addition, all prepared dispersions exhibited a shear-thinning behaviour as well as an increase in shear-yielding stress from 0.90 Pa to 794.5 Pa with increasing PEDOT:PSS concentration from 10 mg mL^{-1} to 50 mg mL^{-1} (Figures S4 and S5). For dispersions with low concentration (10 to 50 mg mL^{-1}), the 3D printed ink would spread laterally on the substrate upon printing because of the low viscosity and yield stress. However, the use of concentration of PEDOT:PSS above 100 mg mL^{-1} would not continuously flow through an extrusion nozzle resulting in to clogging a printing nozzle (see Figure S5F) due to aggregated PEDOT:PSS (Yuk et al., 2020). The electrical conductivity of the thermocell electrodes is one of the key elements affecting performance (Dupont et al., 2017) It is a clear advantage to use as high a concentration of PEDOT:PSS as possible (Kim et al., 2002;

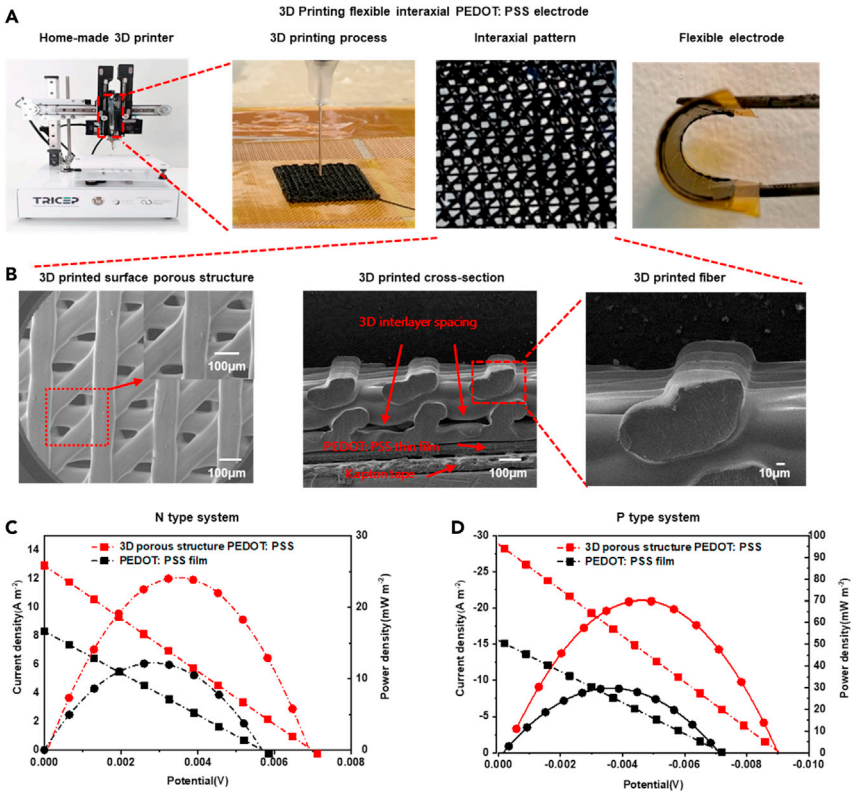

Figure 2. Preparation and characterization of electrodes for p-type and n-type cells

(A) The process of 3D printing flexible interaxial PEDOT: PSS electrode.

(B) Surface and cross-sectional SEM images of printed PEDOT: PSS (scale bar size is 100μm for surface and cross-section, scale bar size is 10μm for 3D printed fiber).

(C) TEC performance: current & power versus voltage of the devices made from 3D porous structured PEDOT: PSS and PEDOT: PSS film in n type system.

(D) TEC performance: current & power versus voltage of the devices made from 3D porous structure PEDOT: PSS and PEDOT: PSS film in p type system.

Tian et al., 2017; Yuk et al., 2020). However, the objective of high electrical conductivity has to be a compromise with processability of the prepared suspensions. Hence, we found that PEDOT:PSS ink with a concentration of 100 mg mL^{-1} which exhibited favourable rheological properties with a viscosity of 15,485 Pa·s at a shear rate of 0.01S^{-1} and shear yield stress of 572 Pa, can be considered as an optimized ink to be processed through extrusion based 3D printing.

3D printed PEDOT:PSS ink on electrical conductive substrates

The prepared ink could be printed via our 3DREDI being manufactured by TRICEP at University of Wollongong (see Figure 2A). As 3D printed patterns can affect the electrical and mechanical properties of final energy devices performance (Li et al., 2020; Wang et al., 2018), a newly interaxial pattern (in this design, the printed direction rotated through 45 degrees for each successive layer) was printed with speed of 200 mm min^{-1} and nozzle size of 0.15 mm were utilized. The designed layer-by-layer printing patterns are shown in Figure S6A with a line spacing of 0.2 mm. The rotating 45° interaxial pattern is designed to create high porosity through both the surface and cross-sections of the multi-layer PEDOT:PSS structure. This is because of the lower electrical resistance resulted from more electrical channels and the robust structure with higher modulus in 3D printed structure with an interaxial angle of 45°(Huang et al., 2018). Figure 2B shows SEM images of 3D printed porous PEDOT:PSS electrode (surface and cross-section). This 3D porous patterned architecture is expected to increase the ionically accessible surface area of the electrode and facilitate the penetration of electrolyte into the active electrode materials. We further compared the TEC performance of PEDOT:PSS film and the 3D interaxial porous PEDOT:PSS electrode in both n and

p type electrolyte systems, Figures 2C and 2D. The PEDOT:PSS film mass loading was 12 mg cm^{-2}. The mass loading of the 3D printed interaxial porous PEDOT: PSS was 10 mg cm^{-2} which was printed onto a 2mg cm^{-2} conductive substrate, so the total 3D interaxial porous PEDOT: PSS electrode is 12 mg cm^{-2}(the mass loading of 1 layer 3D-printed PEDOT: PSS electrode is 1 mg cm^{-2}). Electrolyte systems were p-type: CMC-$K_{3/4}FeCN_6$, and n-type: PVA-$FeCl_{2/3}$, respectively, with a system temperature difference (ΔT) of 10°C (T_H = 35°C & T_C = 25°C). Owing to the open and porous structure (Figure 2B) as well as the good wettability of PEDOT:PSS (Wang et al., 2020), the thermocell made from the 3D printed PEDOT:PSS electrode exhibited an enhanced thermoelectrochemical performance compared to PEDOT:PSS film with increasing current from 8.2 A m^{-2} to 13.0 A m^{-2} and power density from 12.2 mW m^{-2} to 25 mW m^{-2} for n type and 15.2 A m^{-2} to 27.5 A m^{-2} and power density from 30.2 mW m^{-2} to 70 mW m^{-2} for p type (Figures 2C and 2D). In addition, the use of 3D electrodes also increases the open voltage compared to the 2D film electrode from 5.86 mV to 6.90 mV in n type device and from 7.40 mV to 9.21 mV in p type device. This result is because of the 3D porous structure enabling greater heat transfer efficiency from electrode surface to the electrode/electrolyte interface (Liu et al., 2020), and thus the real temperature difference between the cold side and hot side of 3D printed electrode/electrolyte interface is increased.

For long-term current output of both PEDOT:PSS film and 3D porous structure PEDOT:PSS, the short circuit current (I_{soc}) over time was measured and evaluated (Figures S6B and S6C). It was observed that the current output dropped dramatically and stabilized at a value of approximately 1 A m^{-2} after 30 min. This was due to the redox couples' low diffusion rate in gel electrolyte systems (Wu et al., 2017). Owing to the higher driven potential for ion diffusion, the long-term current density of the 3D printed porous PEDOT:PSS electrode was still higher than that of the PEDOT:PSS film electrode (1.25 A m^{-2} versus 1.05 A m^{-2} in n type) and (1.15 A m^{-2} versus 0.94 A m^{-2} in p type). In addition, cyclic voltammograms (CV) with scan rate of 10 mV s^{-1} were performed, where the faradic peak current density provides insight into the electroactive surface area (ESA) of the electrode and could greatly affect the thermocell devices performance (Romano et al., 2013). It is clearly seen that the 3D printed porous structure PEDOT:PSS exhibited higher peak current density than the 2D film under the same mass loading (10 mg cm^{-2}) in both types (Figure S7A for n type and Figure S7C for p type). Table S2 indicates that the 3D porous PEDOT:PSS electrodes could provide larger electroactive surface area than the 2D film electrode so as to enhance the current density.

Electrochemical impedance spectroscopy (EIS) was also performed. The equivalent series resistance (ESR, the intercept of the curve with the x-axis of the Nyquist plot) of 3D porous structure PEDOT:PSS was slightly reduced compared with 2D PEDOT:PSS film in both types (Figures S7B and S7D). These measurements indicate that the 3D porous structure PEDOT:PSS electrode gave the benefit of lowering the activation barrier in thermocell reactions. The improved reaction characteristics also led to the ESR being significantly reduced from 5.4 to 5.2 Ω in n type and from 11.1 to 9.6 Ω in p type as shown in Figures S7B and S7D insert images. In addition, the charge transfer resistance (R_{ct}, the diameter of the semicircle) can clearly be seen for the 3D porous PEDOT:PSS (3.7 Ω) and PEDOT: PSS film (4.32 Ω) in n type; 3D porous PEDOT: PSS (8.1Ω) and PEDOT: PSS film (8.4Ω) in p type, respectively. These observations from EIS agree with the CV results.

Optimizing electrode for both n and p type cells and pairing the optimized n–p cells

Then, we printed various layers of 3D porous PEDOT: PSS on PEDOT: PSS thin film substrate (2 mg cm^{-2}) as electrode materials for both n and p types. In order to improve thermocell performance, we further increased the printed layer of PEDOT:PSS from 10 layers to 30 layers (equals to 10 mg cm^{-2} to 30 mg cm^{-2} of mass loading, electrode thickness in Table S1) to facilitate an increase in electroactive sites (Figure S8A). The thermoelectrochemical performance in n type electrolyte was improved with increasing layers of 3D printed PEDOT:PSS, while it reached a plateau when the number of layers went beyond 20. This was ascribed to the restricted ion penetration into the outer part of electrode materials which was not directly exposed to the electrolyte. In addition, higher layers of electrode also inhibited the effective heat transfer, as indicated by the decreased open circuit voltage. For the long-term performance of the n-type optimized thermocell device (see Figure S8B), the high current output decreased initially, which is a disadvantage of all gel electrolyte based thermocells (Liu et al., 2020). However, it is noted that the 3D printed electrodes optimized for n type thermocells can exhibit a higher long-term J_{SC} (1.65 vs 1.50 A m^{-2}). This represents a 10% improvement upon our previous reported work using laser-etched PEDOT:PSS film as electrode (Liu et al., 2020). Meanwhile, CV curves (scan rate of 10 mv s^{-1}) in Figure S8C also clearly indicate the best electroactive properties of the 20-layer PEDOT:PSS electrode. Electrochemical impedance spectroscopy (EIS) was also carried out in the n-type electrolyte, where it was clearly found

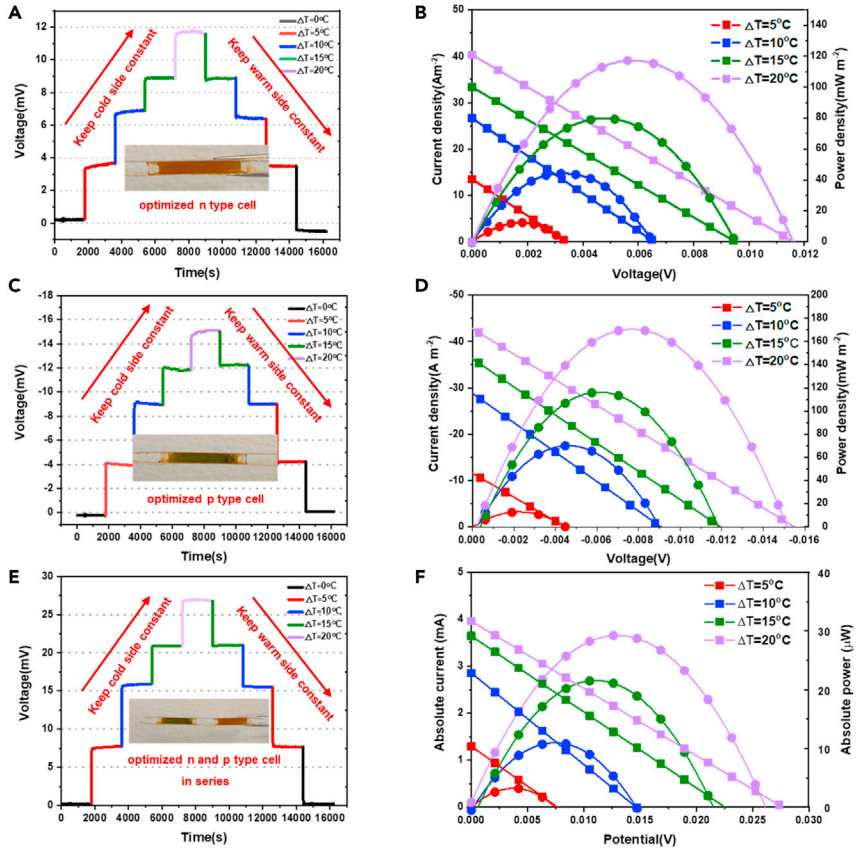

Figure 3. TEC performance: current & power versus voltage of optimized p–n cell at different ΔT

(A) and (B) optimized n type TEC performance at different ΔT.

(C) and (D) optimized p type TEC performance at different ΔT.

(E) and (F) optimized n and p types connected in series TEC performance at different ΔT.

that the ESR was significantly reduced from 6.37 Ω (2 mg cm^{-2} PEDOT:PSS film) to 5.13 Ω (20 layers of 3D printed PEDOT:PSS on top of PEDOT:PSS thin film), denoted as 20-layer PEDOT:PSS) (Figure S8D inset). The Nyquist plot also shows that the charge transfer resistance (the diameter of the semicircle) of 4.16 Ω and 5.3 Ω for 20-layer PEDOT:PSS and 2 mg cm^{-2} PEDOT:PSS film. These observations from EIS and CV are consistent with the results of the thermoelectrochemical performance. Therefore, 20-layer PEDOT:PSS is the optimized electrode for n-type thermocells.

After the optimization for n-type thermocells, thermoelectrochemical performance of 3D printed electrodes in p-type gel electrolytes were also investigated. It was found that 10 layers of PEDOT:PSS on 2 mg cm^{-2} PEDOT:PSS film exhibits the best performance (Figure S9A). The current density was also improved by 11% (1.26 vs 1.13 A m^{-2} in Figure S9B) when compared to our previously reported PEDOT:PSS-edge functionalized graphene/carbon nanotube electrode (PEDOT: PSS/EFG/CNT)(Liu et al., 2020). CV and EIS results also confirmed 10-layer PEDOT: PSS as the optimized electrodes with highest electroactive behaviour and lowest resistances (*i.e.*, ESR & charge transfer resistance), as shown in Figures S9C and S9D.

The thermoelectrochemical performance of thermocell devices is greatly dependent on the temperature difference between the two electrodes, so the devices were tested under various ΔT (Dupont et al., 2017). Here, the cold side or the warm side was kept constant as 10°C or 30°C respectively, and then the other side increased from 10°C to 30°C or decreased from 30°C to 10°C to create controlled ΔT's in the range of 0°C to 20°C. The open voltage of the optimized n and p type cells increased or decreased almost linearly with ΔT (Figures 3A and 3C). Thus, the effective S_e of n and p type cells was calculated to be 0.65 mV K^{-1} and 9 mV K^{-1}, respectively. Current density also increased linearly with ΔT, whereas power density has

a linear relationship with $(\Delta T)^2$ as shown in Figures 3A, 3C, and 3D, which indicates that the individual optimized n and p cells were stable at various temperature gradients.

When multiple cells are assembled into a series circuit, the current output is rate limited by the individual cell with the least performance and the open voltage is the sum of all the individual cells (Yang et al., 2016). To effectively connect the n type and p type thermocells in series, single devices with similar current output should be matched for one pair of n-p thermocells. We found that, our optimized n type and p type cells just in line with this requirement with comparable current densities of 26.1 A m^{-2} and 27.5 A m^{-2} at ΔT = 10°C respectively, and therefore were selected for a matched n-p thermocells (Figures 3B and 3D). Thus, a pair of n–p cells connected in series was fabricated (Figure 3E insert) and the thermoelectrochemical performance characterized (Figures 3E and 3F). The n-p cell performance between ΔT's of 5–20°C were examined, yielding linear V versus I and parabolic P versus V relationships at all temperature differences. The n-p cell exhibited current density of 26.0 A m^{-2} and open circuit voltage of 15.5 mV at ΔT = 10°C, where the current density is same with n and p type single devices and the voltage value is the sum of n and p type single cells (Figure S10A). In addition, long-term output current of the n-p cell was consistent with that of the individual optimized n type and p type. All the results demonstrate the efficient matching of the optimized n and p type devices for n-p cells (Figure S10B).

Prototyping multiple n–p cells

To further promote application, flexible multi- n-p cell assemblies (up to 18 pairs) were fabricated as shown in Figures 4A and 4B. To facilitate the heat transfer between the assembled device and the environment, polyimide tape (PI), the support substrate used for PEDOT:PSS electrode, was adhered to aluminium foil. Sputter coated Pt was used as the interconnection between single devices and copper tape was used to connect multiple n-p cells to external electrical connections. Wearable polydimethylsiloxane (PDMS, SE 1700 clear base and catalyst) was 3D-printed as the spacer to encapsulate the gel electrolyte. The power density of the multi-cell arrangement was measured and found to increase from 10.5 μW (1 pair) to 45 μW (18 pairs) at ΔT = 10°C. The open voltage also increased from 15.5 mV (1 pair) to 270 mV (18 pairs) (Figures 4C and S10C). However, because of the increased resistance between fabricated thermocell connections, the current output inevitably decreased when the number of n-p pairs increased (see Figure S10C). These n-p cell arrays could charge up various commercial electrochemical supercapacitors (C = 1, 4.7, 22, 47, and 100 mF) to more than 200 mV (see Figure 4D). It was also observed that due to the relatively decreased long-term performance of our thermocells employing gel electrolyte, the charging rate of supercapacitors (C = 100 mF) decreased along with time. Notably, this is the first time that a flexible thermocell device has been fabricated using the 3D printing of all polymer electrodes.

Wearable n-p cells

To harvest body heat, a wearable thermocell that can conform to a curved body surface is preferred. To achieve this aim, we designed a strap shaped wearable thermocell as shown in Figure 5A. The fabricated device is shown in Figure 5B. The benefit of this design is that the top electrodes of the wearable strap shaped thermocell could move freely so that the strap arrangement could bend around the contours of the wearer. This ensured that the bottom electrodes of the device could conform closely to the skin of the wearer (Figure 5C). As a demonstration (Figure 5D), we have attached the strap shaped thermocell array to a human body. The wearable thermocell could charge up a 100 mF supercapacitor, and then power a lab timer when coupled with a voltage booster. The results indicated the practical application of our wearable thermocells in powering wearable electronics utilizing low grade human body heat.

Conclusions

In conclusion, we have fabricated novel wearable multi-unit thermocells assembly through 3D-printing all polymer-based flexible electrodes. We also matched serial thermocells and brought about an open voltage of 0.27 V to charge up a supercapacitor and store the harvested energy when operating with a ΔT = 10°C. Moreover, the demonstration of a wearable thermocell, which can harvest body heat, charge commercial supercapacitors, and even power a lab timer, shows the great potential of our wearable device in practical applications. This work provides a platform for the future development of 3D-printable integrated wearable device systems.

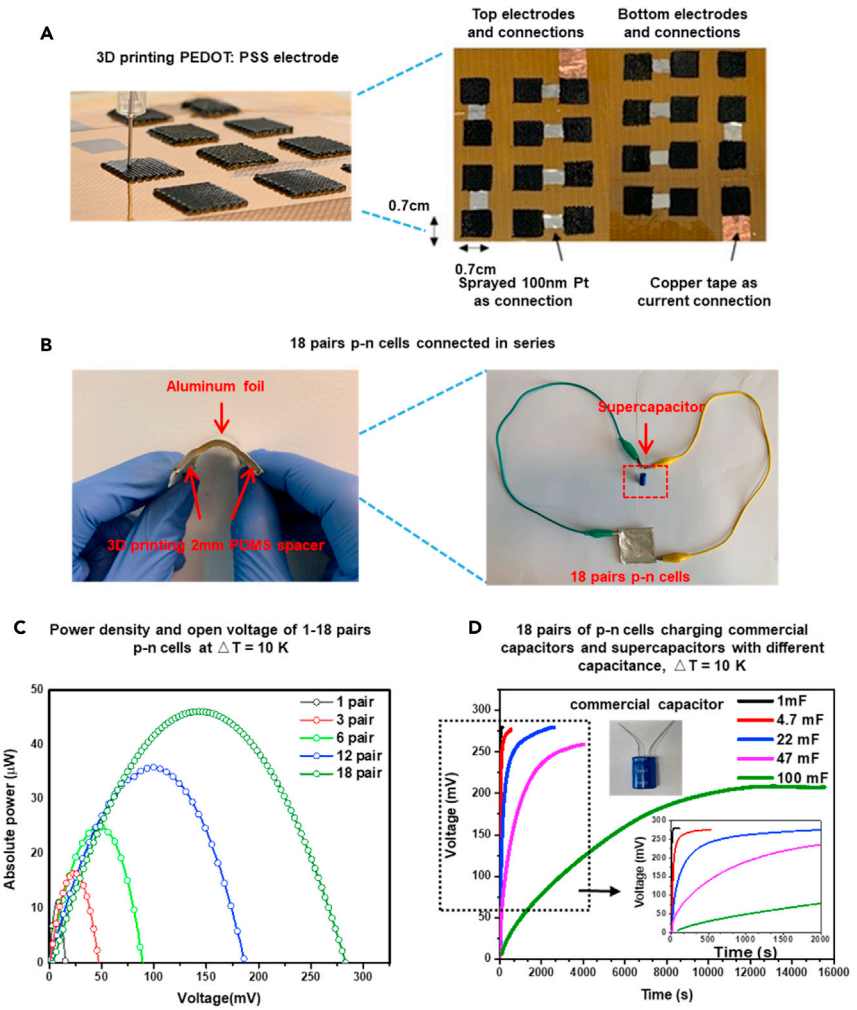

Figure 4. Device evaluation of p-n cells connected in series

(A) Photo demo of thermocell arrays with serial 6 pairs n-p cells.

(B) Prototyping thermo-electrochemical device of 18 pairs n-p cells.

(C) When ΔT = 10°C, 1 to 18 serial pairs of n-p cells TEC performance and

(D) 18 serial pairs of n-p cells charging up commercial super-capacitors with different capacitance.

Limitations of the study

Compared with previous thermocells, the polymer wearable thermocells developed in this work have the following advantages. First, a compatible high electrical conductivity polymer film can work as an underlying conductive substrate, to replace traditional and expensive platinum electrodes. Second, a 3D printable polymer ink with suitable rheological properties was developed for high-performance electrodes in both n and p type thermocell devices, which enables facile and cost-effective fabrication of thermocells. Thirdly, a serial arrangement of 18 pairs of n-p devices enabled charging of commercial supercapacitors up to 0.27 V sufficient to power a commercial lab timer. Last but not least, we also claim that this is the first time that a 3D-printed all-polymer electrode thermocell device was utilized for harvesting body heat. Despite this progress, we note the need for further optimizations of our printing system. It is necessary to develop printing techniques with a high resolution of minimum feature size down to 10 μm in the future, which can further increase the porosity and surface area of electrode materials. Furthermore at present, only inks of electrode materials are developed in this work. In the near future, it is urgent to develop inks consisting of other components (e.g., electrolyte & encapsulation materials). Fully integrated manufacturing requires multi-materials dispersion approaches.

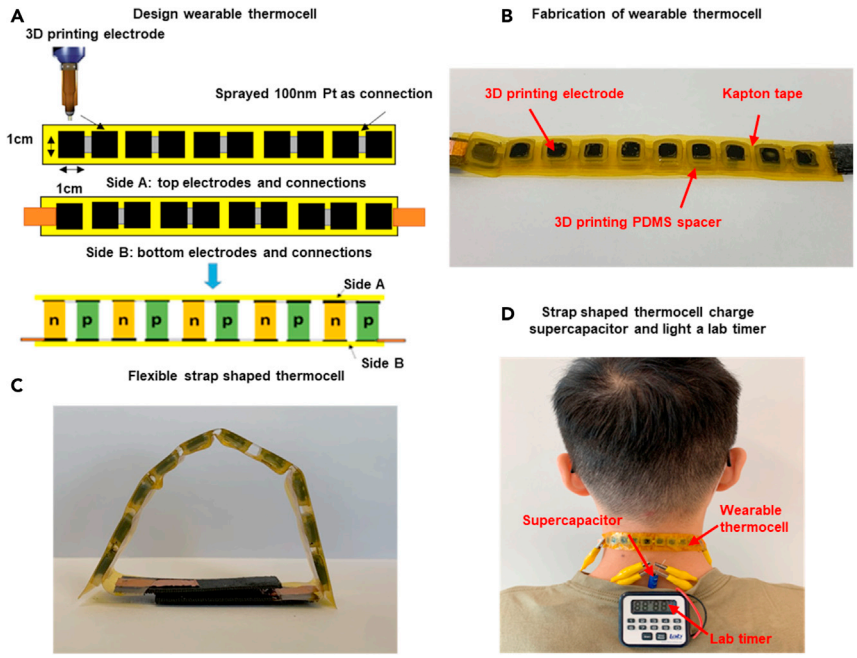

Figure 5. Wearable n-p cells

(A) Design of wearable thermocell.

(B) Fabrication of wearable thermocell.

(C) Flexible strap shaped thermocell.

(D) The demonstration of a strap shaped thermocell charge supercapacitor and light a lab timer screen utilizing body heat.

STAR★METHODS

Detailed methods are provided in the online version of this paper and include the following:

- KEY RESOURCES TABLE
- RESOURCE AVAILABILITY
  - Lead contact
  - Materials availability
  - Data and code availability
- METHOD DETAILS
  - Materials
  - Preparation of gel electrolytes
  - Preparation of electrode ink
  - Rheological characterization of electrode ink
  - 3D printing interaxial pattern electrode
  - Preparation of 3D printable polydimethylsiloxane (PDMS) spacer
  - Device assembly of serial connected thermo-electrochemical cells
  - Cyclic voltammetry (CV)
  - Electrochemical impedance spectroscopy (EIS)
  - Thermo-electrochemical measurements
  - Physical characterizations
- QUANTIFICATION AND STATISTICAL ANALYSIS

SUPPLEMENTAL INFORMATION

Supplemental information can be found online at https://doi.org/10.1016/j.isci.2021.103466.

ACKNOWLEDGMENTS

This study was financially supported by the Australian Research Council Center of Excellence Scheme (Nos. DP170102320 and CE 140100012). Y.L. would like to acknowledge the National Natural Science Foundation of China (No. 52002050 and U20A20338). The authors would like to extend their gratitude to the Materials Node of the Australian National Fabrication Facility.

AUTHOR CONTRIBUTIONS

Methodology, S.Z., Y.Z., Y.L., G.G.W., J.C; Investigation, S.Z., Y.Z., Y.L., J.C; Writing Original Draft, S.Z.; Writing & Review & Editing, S.Z., Y.L., J.C., S.B, G.G.W.; Funding Acquisition, G.G.W., J.C.; Supervision, G.W., S.B., and J.C.

DECLARATION OF INTERESTS

The authors declare no competing interests.

Received: September 23, 2021
Revised: October 19, 2021
Accepted: November 12, 2021
Published: December 17, 2021

REFERENCES

Antiohos, D., Folkes, G., Sherrell, P., Ashraf, S., Wallace, G.G., Aitchison, P., Harris, A.T., Chen, J., and Minett, A.I. (2011). Compositional effects of PEDOT-PSS/single walled carbon nanotube films on supercapacitor device performance. J. Mater. Chem. *21*, 15987–15994. https://doi.org/10.1039/C1JM12986D.

Bux, S.K., Fleurial, J.P., and Kaner, R.B. (2010). Nanostructured materials for thermoelectric applications. Chem. Commun. *46*, 8311–8324. https://doi.org/10.1039/C0CC02627A.

Dupont, M.F., MacFarlane, D.R., and Pringle, J.M. (2017). Thermo-electrochemical cells for waste heat harvesting-progress and perspectives. Chem. Commun. *53*, 6288–6302. https://doi.org/10.1039/C7CC02160G.

Dargusch, M., Liu, W.D., and Chen, Z.G. (2020). Thermoelectric generators: alternative power supply for wearable electrocardiographic systems. Adv. Sci. *7*, 2001362. https://doi.org/10.1002/advs.202001362.

He, Z., Chen, Y., Yang, J., Tang, C., Lv, J., Liu, Y., Mei, J., Lau, W., and Hui, D. (2017). Fabrication of polydimethylsiloxane films with special surface wettability by 3D printing. Compos. Part B Eng. *129*, 58–65. https://doi.org/10.1016/j.compositesb.2017.07.025.

Hu, R., Cola, B.A., Haram, N., Barisci, J.N., Lee, S., Stoughton, S., Wallace, G., Too, C., Thomas, M., Gestos, A., et al. (2010). Harvesting waste thermal energy using a carbon-nanotube-based thermo-electrochemical cell. Nano Lett. *10*, 838–846. https://doi.org/10.1021/nl903267n.

Huang, K., Yang, J., Dong, S., Feng, Q., Zhang, X., Ding, Y., and Hu, J. (2018). Anisotropy of graphene scaffolds assembled by three-dimensional printing. Carbon *130*, 1–10. https://doi.org/10.1016/j.carbon.2017.12.120.

Im, H., Kim, T., Song, H., Choi, J., Park, J.S., Ovalle-Robles, R., Yang, H.D., Kihm, K.D., Baughman, R.H., Lee, H.H., et al. (2016). High-efficiency electrochemical thermal energy harvester using carbon nanotube aerogel sheet electrodes. Nat. Commun. *7*, 10600. https://doi.org/10.1038/ncomms10600.

Im, H., Moon, H.G., Lee, J.S., Chung, I.Y., Kang, T.J., and Kim, Y.H. (2014). Flexible thermocells for utilization of body heat. Nano Res. *7*, 443. https://doi.org/10.1007/s12274-014-0410-6.

Jia, Y., Jiang, Q., Sun, H., Liu, P., Hu, D., Pei, Y., Liu, W., Crispin, X., Fabiano, S., Ma, Y., and Cao, Y. (2021). Wearable thermoelectric materials and devices for self-powered electronic systems. Adv. Mater. *33*, 2102990. https://doi.org/10.1002/adma.202102990.

Kang, T.J., Fang, S., Kozlov, M.E., Haines, C.S., Li, N., Kim, Y.H., Chen, Y., and Baughman, R.H. (2012). Electrical power from nanotube and graphene electrochemical thermal energy harvesters. Adv. Funct. Mater. *22*, 477–489. https://doi.org/10.1002/adfm.201101639.

Khan, Z.U., Edberg, J., Hamedi, M.M., Gabrielsson, R., Granberg, H., Wågberg, L., Engquist, I., Berggren, M., and Crispin, X. (2016). Thermoelectric polymers and their elastic aerogels. Adv. Mater. *28*, 4556–4562. https://doi.org/10.1002/adma.201505364.

Khan, S., Kim, J., Acharya, S., and Kim, W. (2021). Review on the operation of wearable sensors through body heat harvesting based on thermoelectric devices. Appl. Phys. Lett. *118*, 200501. https://doi.org/10.1063/5.0049347.

Kim, J.Y., Jung, J.H., Lee, D.E., and Joo, J. (2002). Enhancement of electrical conductivity of poly(3,4-ethylenedioxythiophene)/poly(4-styrenesulfonate) by a change of solvents. Synth. Met. *126*, 311–316. https://doi.org/10.1016/S0379-6779(01)00576-8.

Li, X., Li, H., Fan, X., Shi, X., and Liang, J. (2020). 3D-printed stretchable micro-supercapacitor with remarkable areal performance. Adv. Energy Mater. *10*, 1903794. https://doi.org/10.1002/aenm.201903794.

Liu, Y., Wang, H., Sherrell, P.C., Liu, L., Wang, Y., and Chen, J. (2021). Potentially wearable thermo-electrochemical cells for body heat harvesting: From mechanism, materials, strategies to applications. Adv. Sci. *8*, 2100669. 1–23. https://doi.org/10.1002/advs.202100669.

Liu, Y., Zhang, B., Xu, Q., Hou, Y., Seyedin, S., Qin, S., Wallace, G.G., Beirne, S., Razal, J.M., and Chen, J. (2018). Development of graphene oxide/polyaniline inks for high performance flexible microsupercapacitors via extrusion printing. Adv. Funct. Mater. *28*, 1–12. https://doi.org/10.1002/adfm.201706592.

Liu, Y., Zhang, S., Zhou, Y., Buckingham, M.A., Aldous, L., Sherrell, P.C., Wallace, G.G., Ryder, G., Faisal, S., Officer, D.L., et al. (2020). Advanced wearable thermocells for body heat harvesting. Adv. Energy Mater. *10*, 2002539. https://doi.org/10.1002/aenm.202002539.

Oh, J.Y., Lee, J.H., Han, S.W., Chae, S.S., Bae, E.J., Kang, Y.H., Choi, W.J., Cho, S.Y., Lee, J.O., Baik, H.K., and Lee, T. Il (2016). Chemically exfoliated transition metal dichalcogenide nanosheet-based wearable thermoelectric generators. Energy Environ. Sci. *9*, 1696–1705. https://doi.org/10.1039/C5EE03813H.

Perinka, N., Kim, C.H., Kaplanova, M., and Bonnassieux, Y. (2013). Preparation and characterization of thin conductive polymer films on the base of PEDOT:PSS by ink-jet printing. Phys. Proced. *44*, 120–129. https://doi.org/10.1016/j.phpro.2013.04.016.

Romano, M.S., Gambhir, S., Razal, J.M., Gestos, A., Wallace, G.G., and Chen, J. (2012). Novel carbon materials for thermal energy harvesting. J. Therm. Anal. Calorim. *109*, 1229–1235. https://doi.org/10.1007/s10973-012-2311-9.

Romano, M.S., Li, N., Antiohos, D., Razal, J.M., Nattestad, A., Beirne, S., Fang, S., Chen, Y., Jalili,

R., Wallace, G.G., et al. (2013). Carbon nanotube-reduced graphene oxide composites for thermal energy harvesting applications. Adv. Mater. *25*, 6602–6606. https://doi.org/10.1002/adma.201303295.

Shi, X.L., Zou, J., and Chen, Z.G. (2020). Advanced thermoelectric design: from materials and structures to devices. Chem. Rev. *120*, 7399–7515. https://doi.org/10.1021/acs.chemrev.0c00026.

Sinha, S.K., Noh, Y., Reljin, N., Treich, G.M., Hajeb-Mohammadalipour, S., Guo, Y., Chon, K.H., and Sotzing, G.A. (2017). Screen-printed PEDOT:PSS electrodes on commercial finished textiles for electrocardiography. ACS Appl. Mater. Inter. *9*, 37524–37528. https://doi.org/10.1021/acsami.7b09954.

Tian, K., Bae, J., Bakarich, S.E., Yang, C., Gately, R.D., Spinks, G.M., in het Panhuis, M., Suo, Z., and Vlassak, J.J. (2017). 3D printing of transparent and conductive heterogeneous hydrogel–Elastomer systems. Adv. Mater. *29*, 1604827. https://doi.org/10.1002/adma.201604827.

Tian, R., Liu, Y., Koumoto, K., and Chen, J. (2019). Body heat powers future electronic skins. Joule *3*, 1399–1403. https://doi.org/10.1016/j.joule.2019.03.011.

Wang, J., Sun, Q., Gao, X., Wang, C., Li, W., Holness, F.B., Zheng, M., Li, R., Price, A.D., Sun, X., et al. (2018). Toward high areal energy and power density electrode for Li-ion batteries via optimized 3D printing approach. ACS Appl. Mater. Inter. *10*, 39794–39801. https://doi.org/10.1021/acsami.8b14797.

Wang, Y., Mukaida, M., Kirihara, K., Lyu, L., and Wei, Q. (2020). Poly(3,4-ethylene dioxythiophene)/poly(styrene sulfonate) electrodes in electrochemical cells for harvesting waste heat. Energy Technol *8*, 1900998. https://doi.org/10.1002/ente.201900998.

Wijeratne, K., Vagin, M., Brooke, R., and Crispin, X. (2017). Poly(3,4-ethylenedioxythiophene)-tosylate (PEDOT-Tos) electrodes in thermogalvanic cells. J. Mater. Chem. A. *5*, 19619–19625. https://doi.org/10.1039/C7TA04891B.

Wu, J., Black, J.J., and Aldous, L. (2017). Thermoelectrochemistry using conventional and novel gelled electrolytes in heat-to-current thermocells. Electrochimica Acta *225*, 482–492. https://doi.org/10.1016/j.electacta.2016.12.152.

Yang, P., Liu, K., Chen, Q., Mo, X., Zhou, Y., Li, S., Feng, G., and Zhou, J. (2016). Wearable thermocells based on gel electrolytes for the utilization of body heat. Angew. Chem. *128*, 12229–12232. https://doi.org/10.1002/ange.201606314.

Yuk, H., Lu, B., Lin, S., Qu, K., Xu, J., Luo, J., and Zhao, X. (2020). 3D printing of conducting polymers. Nat. Commun. *11*, 1604. https://doi.org/10.1038/s41467-020-15316-7.

Zhang, S., Liu, Y., Hao, J., Wallace, G.G., Beirne, S., and Chen, J. (2021). 3D-printed wearable electrochemical energy devices. Adv. Funct. Mater. 2103092. https://doi.org/10.1002/adfm.202103092.

Zhong, J., Zhang, Y., Zhong, Q., Hu, Q., Hu, B., Wang, Z.L., and Zhou, J. (2014). Fiber-based generator for wearable electronics and mobile medication. ACS Nano *8*, 6273–6280. https://doi.org/10.1021/nn501732z.

Zhou, Y., Liu, Y., Buckingham, M.A., Zhang, S., Aldous, L., Beirne, S., Wallace, G., and Chen, J. (2021). The significance of supporting electrolyte on poly (vinyl alcohol)–iron (II)/iron (III) solid-state electrolytes for wearable thermo-electrochemical cells. Electrochem. Commun. *124*, 106938. https://doi.org/10.1016/j.elecom.2021.106938.

STAR★METHODS

KEY RESOURCES TABLE

REAGENT or RESOURCE	SOURCE	IDENTIFIER
Chemicals, peptides, and recombinant proteins		
Poly (3,4-ethylenedioxythio-phene): Polystyrenesulfonate pellets (PEDOT: PSS)	Sigma-Aldrich	Cat# 768618
Diethylene glycol (DEG)	Sigma-Aldrich	Cat# 93171
Poly (vinyl alcohol) (PVA)	Sigma-Aldrich	Cat# 363146
Carboxymethylcellulose sodium (CMC)	Sigma-Aldrich	Cat#419311
Iron (II) chloride tetrahydrate ($FeCl_2 \cdot 4H_2O$)	Sigma-Aldrich	Cat# 44939
Iron (III) chloride ($FeCl_3$)	Sigma-Aldrich	Cat# 157740
Potassium ferricyanide (K_3FeCN_6)	Sigma-Aldrich	Cat# 244023
Potassium hexacyanoferrate (II) ($K_4FeCN_6 \cdot 3H_2O$)	Sigma-Aldrich	Cat# 234125
Glutaraldehyde (GA) solution (25 wt% in H_2O)	Sigma-Aldrich	Cat# G5882
Hydrochloric acid	Sigma-Aldrich	Cat# 320331
Polydimethylsiloxane (PDMS), PDMS (catalyst) SE 1700	Dow Corning Toray Co., Ltd	Cat#0008248086
Software		
TEC Service Software v3.10	Meerstetter Engineering	TEC-1091
Origin 2020	Graphing and data analysis software	https://www.originlab.com/
Adaptable (3D printer interface)	The Translational Research Initiative for Cell Engineering and Printing	https://www.tricep.com.au/
EC-lab software	Bio-Logic	https://www.biologic.net/support-software/ec-lab-software/
Other		
Home-made temperature controller	Liu et al. (2020)	https://onlinelibrary.wiley.com/doi/abs/10.1002/aenm.202002539
3DREDI printer	TRICEP at University of Wollongong	https://www.tricep.com.au/
VSP Potentiostat Electrochemical Workstation	Bio-Logic	https://www.biologic.net/products/vsp/
Lab timer	Labco	LABTR01
Voltage Booster	CUSTOM THERMOELECTRIC	ELC-UVB040 Unipolar
Mixing Thinky	INTERTRONICS	ARE-250
Bandelin sonorex digiplus sonicator	John Morris	J:141375
Vaccum Oven	ISSCO	VDO-30CH
AR G2 Rheometer	TA Instruments	TT016
Sputter Coater	Edwards	FTM6 Auto 306
Optical Microscope	Leica	DM6000
Scanning Electron Microscopy	JEOL	JEOL JSM-7500FA
Spiral micrometer	Mitutoyo	293-831
Microelectrode	Micrux	ED-SE1-Pt

RESOURCE AVAILABILITY

Lead contact

Further information and requests for resources should be directed to and will be fulfilled by the lead contact, Jun Chen (junc@uow.edu.au).

Materials availability

This study did not generate new unique reagents.

Data and code availability

- Original data reported in this paper will be shared by the lead contact upon request.
- This paper does not report original code.
- Any additional information required to reanalyze the data reported in this paper is available from the lead contact upon request.

METHOD DETAILS

Materials

The poly (3,4-ethylenedioxythio-phene): polystyrenesulfonate pellets (PEDOT: PSS, Orgacon DRY product) was purchased from the Sigma-Aldrich(768618). Diethylene glycol (DEG), poly (vinyl alcohol) (PVA, Mw: 85,000–124,000), Carboxymethylcellulose sodium (CMC, Mw: 250,000), iron (II) chloride tetrahydrate ($FeCl_2{\cdot}4H_2O$), iron (III) chloride ($FeCl_3$), potassium ferricyanide (K_3FeCN_6), potassium hexacyanoferrate (II) ($K_4FeCN_6{\cdot}3H_2O$), glutaraldehyde (GA) solution (25 wt% in H_2O), Hydrochloric acid was from Sigma-Aldrich. Polydimethylsiloxane (PDMS, SE 1700) and PDMS catalyst were purchased from Dow Corning Toray Co., Ltd. The operating voltage of lab timer is 1.5v, voltage Booster was purchased from CUSTOM THERMOELECTRIC (ELC-UVB040 Unipolar Voltage Booster).

Preparation of gel electrolytes

N type electrolyte: PVA solution of 10 wt% was first prepared, then adding $FeCl_2{\cdot}4H_2O$ and $FeCl_3$ powder (1 M $FeCl_{2/3}$) with magnetic stirring) for 1 h. The chemical cross-linker of diluted GA (5 wt% in H2O, mass ratio of PVA: GA = 40:1) was then dropped carefully into the mixed solution with vigorous magnetic stirring for 30 s. After that, the PVA-$FeCl_{2/3}$-GA solution was immediately injected into the assembled thermoelectrochemical device. Finally, the solid-state gel electrolyte could form after cross-linking at room temperature for 1 h (Liu et al., 2020).

P type electrolyte: CMC-$K_{3/4}Fe(CN)_6$ gel electrolyte was prepared as following: 5wt% of CMC powder was adding into 0.4 M $K_3Fe(CN)_6/K_4Fe(CN)_6$ aqueous solution with magnetic stirring 4h before injecting into thermoelectrochemical devices for p type performance testing (Liu et al., 2020).

Preparation of electrode ink

Firstly, DEG was added to the DI water, stirred 20 min and sonicated for 30 min. To prepare PEDOT: PSS printable ink, commercial PEDOT: PSS pellets (50 to 600 mg), water (5 mL), DEG (83 to 996 ul) was mixed by Thinky Mixer for 20 min, 2000 rmp and degassing for 2 min, 800 rmp (weight ratio of DEG: (PEDOT: PSS) = 1.86:1). Then, the prepared ink was carefully transferred to the syringe for printing.

Rheological characterization of electrode ink

In this work, an AR G2 Rheometer (40-mm diameter geometry and cone truncation 55 μm) was used to measure the viscosity (η) of PEDOT: PSS ink for extrusion printing. The sample volume for measurement is 0.5 mL and the shear rate was set from 0.01 to 10 s^{-1}. At 1 Hz shear frequency, the shear storage modulus (G′) and loss modulus (G″) were measured as a function of shear stress via oscillation tests with a logarithmic sweep of shear stress (0.001–10,000 Pa). The shear yield stress of each sample was determined as the intersection point of shear storage modulus (G′) and loss modulus (G″).

3D printing interaxial pattern electrode

The prepared PEDOT: PSS ink can be printed via our 3D printer (see Figure 2A) with printing speed of 200 mm min^{-1}, nozzle size of 0.15 mm (from Nordson EFD), and extrusion pressure of 688 kPa. The G code of printing paths were generated by a 3D printing software (Adaptable, made by Translation Research Initiative of Cellular Engineering and Printing (TRICEP) a wholly owned initiative of the University of Wollongong) to command the three x-y-z motions. Line spacing is 0.2 mm and rotating angle is 45° when increasing every printing layer (Figure S6A). PEDOT: PSS were printed at room temperature, and then heating in 60°C oven for 2h to fully remove DEG.

Preparation of 3D printable polydimethylsiloxane (PDMS) spacer

Polydimethylsiloxane (PDMS) SE 1700 clear base and SE 1700 catalyst was mixed with volume ratio of 10:1(He et al., 2017), following by mixing in Thinky for 5 min, 2000 rmp and degassing 2 min, 800 rmp. The homogenous ink can be printed on PI (kapton tape) with 2 mm as spacer, then heated in 60°C oven 2 h for curing which will be used for further assembly of sandwich device and wearable device fabrication.

Device assembly of serial connected thermo-electrochemical cells

A serial connected thermocell device (interconnected n-type & p-type devices) was fabricated. Firstly, according to designed patterns, we used polyethylene terephthalate (PET) film as mask and sputter coat 100 nm Pt (using an EDWARDS sputter coating machine) on polyimide tape (PI) substrate (fixed on aluminum foil), sprayed Pt acts as connecting lines between individual n and p type devices and copper tape works current collectors. Then, PEDOT: PSS film electrodes were drop-casted on the PI according to the design, following by 3D printed PEDOT: PSS (Figure 4A) on their surfaces. The PDMS was then printed on the edge of electrode and sealed by heating 60°C for 2 h. Finally, n and p type gel electrolyte precursors were injected into the 3D printed thermocells through heat-cured PDMS to form full thermocells (Figure 4B).

Cyclic voltammetry (CV)

CV was recorded by VSP potentiostat (Bio-logic) and EC-lab software (11.21). A conventional three-electrode cell was used for all electrochemical experiments that complemented measurements for the thermocell. The two working electrodes were connected to thermocell electrodes, the reference electrode was platinum wire inserted in n-type gel electrolyte (PVA-$FeCl_{2/3}$) or p-type gel electrolyte (CMC-$K_{3/4}Fe(CN)_6$). CV measurement was measured from −0.8 V to +0.8 V at a scan rate of 10 mv s^{-1}.

Electrochemical impedance spectroscopy (EIS)

EIS was completed using VSP potentiostat (Bio-logic) and EC-lab software (11.21) and measured in the frequency range of 100 kHz-10 mHz with an AC amplitude of 10 mV.

Thermo-electrochemical measurements

Home-made temperature controller were made by our previous work (Liu et al., 2020).

Physical characterizations

Surface porous pattern and the cross-section morphology of 3D porous PEDOT: PSS were investigated with JEOL JSM-7500FA field emission SEM (the acceleration voltage of 5.0 kV, emission current of 10 mA). Surface morphology of pristine PEDOT: PSS thin film, Pt, bended PEDOT: PSS thin film and bended Pt were investigated by Leica DM6000 Optical Microscope. Serial connection Platinum (Pt) was coated by Edwards Sputter Coater. Thickness of various electrodes were measured by Mitutoyo spiral micrometer.

QUANTIFICATION AND STATISTICAL ANALYSIS

Our study does not include statistical analysis or quantification.